Ultramicroscopy 266 (2024) 114021

Contents lists available at ScienceDirect

Ultramicroscopy

journal homepage: www.elsevier.com/locate/ultramic

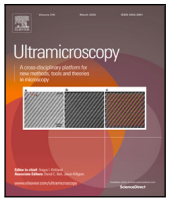

Autoencoder latent space sensitivity to material structure in convergent-beam low energy electron diffraction

M. Ivanov, J. Pereiro *

School of Physics and Astronomy, Cardiff University, United Kingdom

ARTICLE INFO

Dataset link: https://doi.org/10.17035/cardiff.26652991

Keywords:
Low energy electron microscopy
Low energy electron diffraction
Machine learning
Data analysis
Autoencoders
Electron microscopy

ABSTRACT

The convergent-beam low energy electron diffraction technique has been proposed as a novel method to gather local structural and electronic information from crystalline surfaces during low-energy electron microscopy. However, the approach suffers from high complexity of the resulting diffraction patterns. We show that Convolutional Autoencoders trained on CBLEED patterns achieve a highly structured latent space. The latent space is then used to estimate structural parameters with sub-angstrom accuracy. The low complexity of the neural networks enables real time application of the approach during experiments with low latency.

1. Introduction

Low-energy electron microscopy (LEEM) is an established technique in the field of Material Science that uses electrons in the range of 0 eV *to* 100 eV. The shallow electrons penetration depth of a few atomic layers lead to a high surface sensitivity. In crystalline samples, LEEM is accompanied by its complementary technique for surface reconstruction characterisation — low-energy electron diffraction (LEED), which obtains structural information at the crystalline surface by accessing reciprocal space. Varying the energy in that range produces intensity-voltage $I(V)$ curves, giving a comprehensive view of the electron band structure at the surface of a crystalline sample. As the electron beam normally illuminates a large portion of the surface simultaneously, this information is convoluted over that surface. To extract structural information for a spatially localised region of interest, the micro-LEED technique is usually employed, where LEED is routinely used along with a small and well-positioned aperture, which limits the illumination of the surface to patches with diameters of down to 10 μm.

While the micro-LEED technique gathers information using planar-wave electron beams of normal incidence, Held et al. observed that having a beam approach the surface at different angles results in significant intensity modulations in the LEED pattern and enables the gathering of beam-rocking curves, allowing for the analysis of diffraction with respect to the angle of incidence and providing information about the orientation of the crystallographic planes [1]. Spence et al. built on the same concept, suggesting the convergent-beam low energy electron diffraction (CBLEED) technique, where the converging beam geometry has multiple beams approaching the same spot at different angles, replicating the rocking curve output, but from a significantly smaller incidence area [2].

The idea of convergent electron beams has been explored in the past [3]. In practice, convergent-beam electron diffraction (CBED) has been extensively developed in the context of transmission electron microscopy (TEM) [4–12]. Over the years, the TEM-based CBED has been utilised in various applications to a significant impact, such as characterising crystal defects [13], lattice polarity determination [14,15], lattice misfit measurement [16], charge-density distribution mapping [17], measuring strain fields [18] and more. Although CBED is a very versatile approach, it predominantly examines the bulk of crystalline samples, and the relatively high beam irradiation on the sample during TEM, and especially with CBED, is still a challenging problem for imaging beam-sensitive materials [19].

Applying convergent beam in LEED in analogy with CBED through the CBLEED technique mitigates these limitations due to the shallow penetration depth and the sample-preserving nature of the low energy electrons. These benefits allow the gathering of detailed structural information from the surface from localised regions down to several nm in diameter, much smaller than the minimal region diameters of 250 nm in micro-LEED imaging [20]. Similarly to the adoption of convergent beam in TEM, utilising convergent beam in LEEM can open up a new set of applications for the microscope, such as allowing structural analysis of nanostructures on the surface and enabling a scanning mode for the LEEM system for gathering localised structural information.

* Corresponding author.
E-mail address: PereiroViterboJ@cardiff.ac.uk (J. Pereiro).

https://doi.org/10.1016/j.ultramic.2024.114021
Received 14 May 2024; Received in revised form 25 July 2024; Accepted 1 August 2024
Available online 6 August 2024

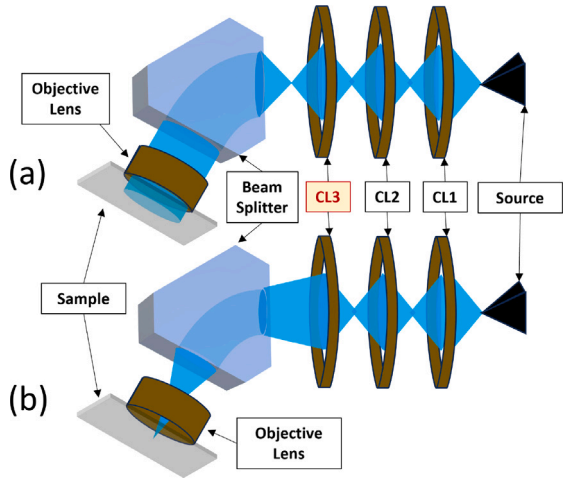

Fig. 1. Convergent beam formation through modifying the LEEM illumination column configuration. The last condenser lens (CL3) can be used to have the beam converge at a point in the sample. A more complete representation of the LEEM lens system can be seen in [22].

To make the application of CBLEED more functional and seamless, we demonstrate a method for the analysis and interpretation of the complex and abstract CBLEED patterns. With this, we aim to help streamline the adoption of the powerful experimental technique. While limited published research based on experimental CBLEED patterns can be found in the literature, the patterns are experimentally achievable [21]. The results presented here aim to increase confidence in the potential of the CBLEED technique by reducing the analysis barrier associated to it. Efficient and accurate extraction of insight from CBLEED patterns can allow more effort and investment in the development of specialised instrumentation to enable the analysis of nanostructures.

We show that a machine learning (ML) approach is able to learn and identify key surface structure properties based on the observed CBLEED pattern. We propose a tool, which enables an automated real-time read of CBLEED patterns through the joint use of a deep learning autoencoder-based (AE) architecture and a simpler ML model. This serves to efficiently inform the researcher during an experiment, making it a more controlled and explainable process. Furthermore, the relatively inexpensive and quick analysis gives a valuable pointer towards the appropriate structures that were observed, mitigating the need for guesswork and exploration of possible structures when experimental data is fitted with simulations. The approach increases the quality of the extracted information from an experiment and mitigates the need for intensive and expensive computation in order to understand the data after its acquisition.

2. Overview

The subject of CBLEED patterns has so far been primarily approached through scattering simulations. Spence et al. demonstrated the equivalence of CBLEED to the information from a conventional I-V curve [2]. The individual LEED spots convolute into disks on a CBLEED pattern, as shown in Fig. 1. There, multiple scattering calculations in metals were used to show the effectiveness and sensitivity of the approach to the surface potential.

Ruben et al. provided a basis for simulating CBLEED patterns on crystalline surfaces [23]. Through kinematic single electron scattering simulations, they showed the sensitivity of the CBLEED pattern to different surface reconstructions and atomic displacements in Si(001) and established the structural sensitivity of CBLEED patterns. Constantinou et al. performed more sophisticated multiple scattering simulations, which yield much more accurate variations in CBLEED pattern intensities in response to small atomic displacements [21].

The outlined current progress in the research on CBLEED patterns provides computational methods of reaching a CBLEED pattern from a determined structure and electron energy, which ripens the field for new data-driven approaches. The currently available method for experimental data interpretation is the traditional brute force approach of producing a range of patterns and matching with experimental ones. Unfortunately, the cost of the brute-force approach scales sharply with the complexity of the examined material, where the variational space quickly becomes large. Furthermore, the convoluted and abstract nature of the patterns does not allow manual interpretation, by eye, of a pattern by a researcher. This makes the practical application of the CBLEED technique quite difficult and expensive. On the other hand, the availability of simulated CBLEED data enables a data-centric statistical approach of analysing CBLEED patterns using Machine Learning.

Machine Learning and Deep Learning algorithms have recently been showing a lot of promise and prowess in their applications on microscopy data across a variety of microscopy imaging techniques [24]. In particular, ML algorithms have been successful in their application in interpreting a variety of diffraction imaging data, such X-ray diffraction [25–29], reflection high-energy electron diffraction [30,31], electron backscatter diffraction [32], scanning precession electron diffraction [33] and more. In particular, we approach the problem of CBLEED pattern analysis using a convolutional neural network-based (CNN) AE architecture. The AE architecture was recently used in the analysis of X-ray diffraction patterns [34,35]. Additionally, the speed and ability of CNN-based networks for extraction of physical parameters, have recently been demonstrated in the close context of CBED by Xu et al. and Zhang et al. [36,37].

3. Methods

3.1. Dataset

The CBLEED dataset we use is generated by Constantinou textitet al. through multiple scattering simulations of patterns on Si(001) [21]. The simulations adapted the CAVATN package, which is based on the CAVLEED program [38]. The simulations for the images used here were performed on the symmetric-dimer and buckled-dimer (2×1) structures. The electron incidence energy was varied between $30\,\mathrm{eV}$ *to* $100\,\mathrm{eV}$ and a range of dimer displacements were introduced to generate a total of about 5000 images in the dataset, examples of which are shown in Fig. 2.

3.2. Model training

For this work, we utilise an autoencoder-based architecture to capture the semantics of the data. AE networks are a type of neural network techniques that learns how to compress and reconstruct high-dimensional data in an *unsupervised* manner. In an autoencoder, the input data is first encoded into a low-dimensional representation, also known as the *latent space*, by a series of non-linear transformations through a set of encoder layers. This latent representation is then decoded back to the original high-dimensional space by a series of decoder layers, producing a reconstruction of the input data. The key feature of an autoencoder is the size of its latent space that is normally significantly smaller that the size of the input data, thus containing much less information. By reconstructing the data from such a concise latent space representation, the training process optimises the utilisation of the limited latent space information capacity. During the training process, the network learns to distil the most significant features of the data, organising them into a structured and compact format within the latent space. Since the input data is in the form of images, the encoder and decoder networks in our architecture are constructed from convolutional layers, followed by a group of fully connected layers and the two networks mirror each other. The full deep convolutional autoencoder (DCAE) architecture is shown in Fig. 3.

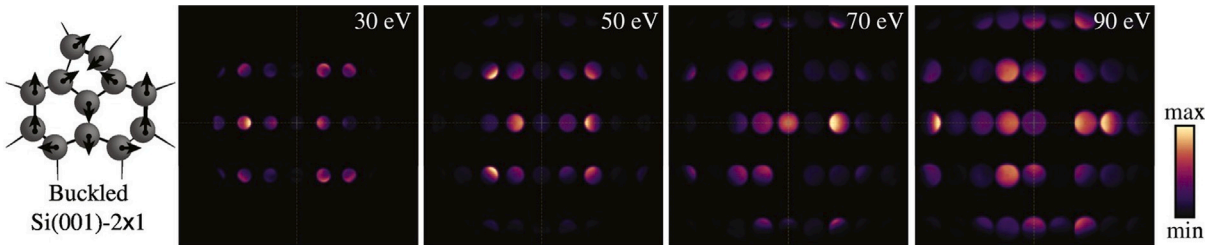

Fig. 2. Examples from the CBLEED dataset. The dataset was generated by introducing sub-angstrom dimer displacements along the dimer-height and dimer-length, relative to a symmetric-dimer Si(001) - (2×1) structure.
Source: Adapted from Constantinou et al. [21].

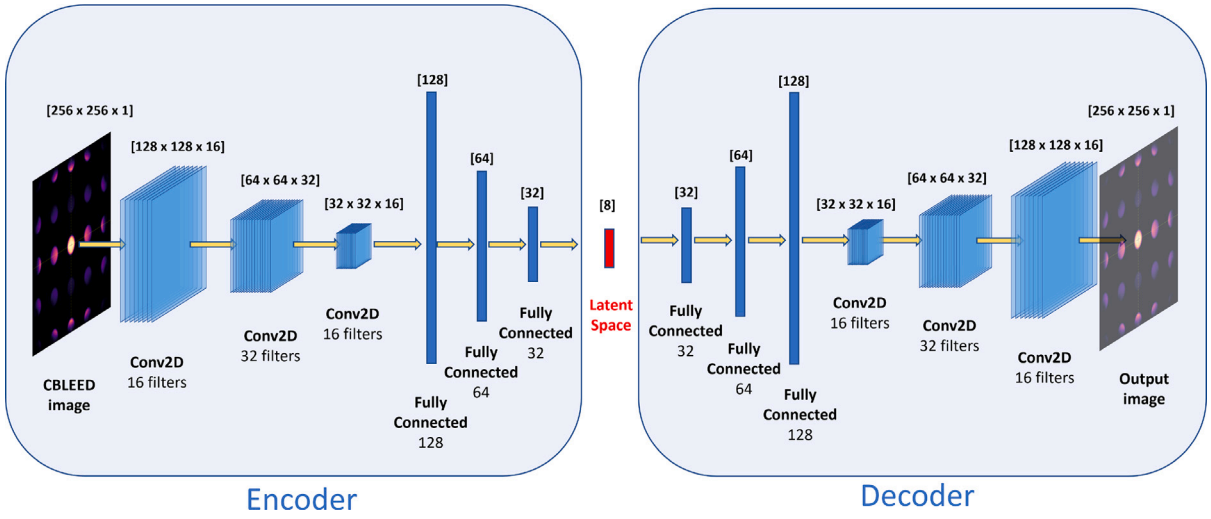

Fig. 3. Deep Convolutional Autoencoder architecture. All convolutional layers apply "Same" padding, a kernel stride of 1. The encoder convolutions are followed by a MaxPooling layer and the decoder convolutions are followed by an UpSampling layer.

The encoder and decoder networks are trained simultaneously using backpropagation to minimise the difference between the input and output. This reconstruction goal is measured using binary crossentropy (BCE) loss. BCE is used over simpler loss functions, such as the mean absolute error (MAE) and mean squared error (MSE), as it generally has the subtle advantages of better preventing loss saturation and also of being a convex function. Examples of the reconstructive ability progress of the DCAE network during its training are shown in Fig. 4.

A consequence of the data flow and a key feature during autoencoder learning is that the data must be squeezed through the bottleneck of the small latent space without losing its essential features. As a result, the latent space needs to act as a compressed representation of the input data that preserves the important information while discarding the redundant or irrelevant information.

4. Analysis

The compressed representation property of the latent space in the autoencoder can be used to extract valuable information from the CBLEED pattern images by providing a compressed, lower-dimensional representation that captures the essential features of the patterns. By exploring the latent space structure, we can identify patterns, trends and clusters of similar data points which are not apparent in the original images. This can give insights onto the parameters of the structure, which produced the corresponding CBLEED pattern. With that in mind, the size of the latent space becomes the most important hyperparameter in our AE architecture for the task.

4.1. Latent space size

To get the most out of the latent space, its size must be carefully chosen. While too small of a latent space will contain too little information and may start losing valuable information, too large of a latent space will hold too much information, lose its generalisation of the data and start overfitting. To find the latent space size with best trade-off, networks with a variety of latent space sizes are trained. Their loss values correspond directly to the quality of the reconstructions they achieve and are therefore an indirect measurement of how successful the latent spaces are in preserving information from the original data. The losses during training of these networks is shown in Fig. 5. As can be seen in the network training converges after a latent space of size 8. This suggests that 8 dimensions in the latent space are just enough to encompass all the needed information from the data, and are most likely to result in the best generalisation of the data. Larger latent spaces do not bring reconstruction improvements and merely contain the same information within a larger latent space, going away from the best generalisation of the data.

4.2. Latent space structure

The CBLEED patterns in the data have been generated by traversing two physical parameters — the beam energy and the dimer displacement, with a step of 1 eV and 0.1 Å respectively. Note that the beam energy is usually a known variable during an experiment, but is kept as a parameter to showcase the ability of the proposed algorithm to generalise multiple physical parameters simultaneously without prior knowledge of them. Hence, the two parameters used for the generations can be considered metadata, which is not accessible to the AE algorithm

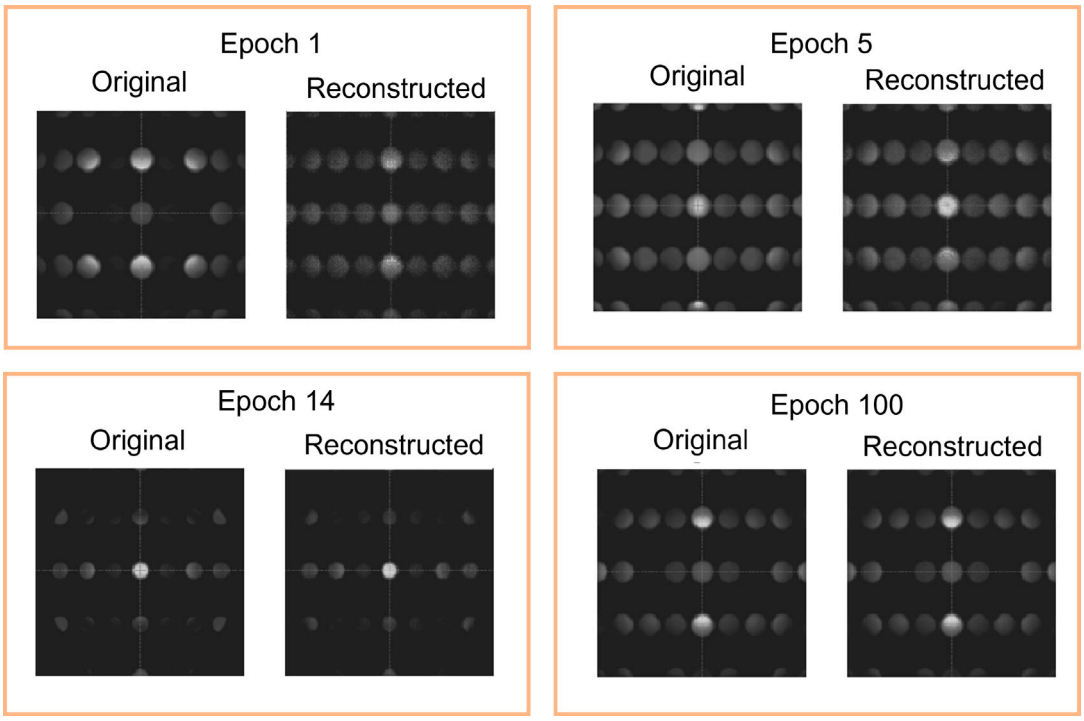

Fig. 4. Autoencoder reconstructions at different training epochs. The reconstructions of the data examples get progressively more accurate and sharper with each iteration over the dataset during training.

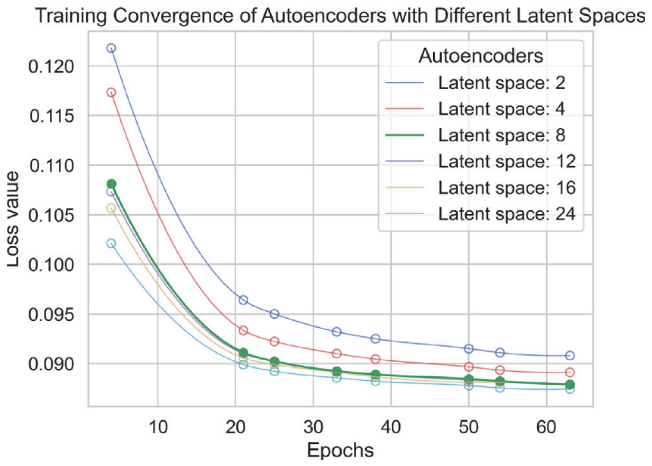

Fig. 5. Training loss of autoencoders with different latent space sizes. The AE architecture between the separate training sessions stays the same, but the dimensionality of the latent space is varied between 2- and 24-dimensional. While the 2- and 4-dimensional AE variations even out at a higher loss, the variations with 8 dimensions and above converge around the same reconstruction loss.

at any time. In order to explore the effectiveness of the latent space generalisation of the CBLEED data, we visualise the projections of each CBLEED pattern in the latent space, labelled with its beam energy and dimer displacement parameters. The structure of the optimal 8 node latent space after training is shown in Fig. 6, where we see how the data is ordered internally when compressed into the latent space. The parameter-based colouring is indicative that the structure of the latent space encoding follows the underlying parameters of the data very well. This suggests the autoencoder latent space learns a good generalisation of the data that can be traced back to the initial data generation process and parameters, without any prior knowledge of them.

Table 1
Comparison of the predictive success of different ML algorithms. Trained and tested on the latent space projections of the training and testing subsets of the dataset, respectively.

Algorithm	Beam energy		Dimer Displ.	
	MAE	R^2	MAE	R^2
KNN	**0.43**	**0.999**	0.025	0.992
RBF SVM	0.83	0.995	0.050	0.978
NuSVM	0.92	0.994	**0.010**	**0.997**
DecisionTree	0.85	0.995	0.024	0.980
ExtraTree	0.87	0.997	0.028	0.973
XGBoost	0.75	0.998	0.028	0.986

4.3. Latent space parameter extraction

We use the trained and structured latent space to extract the parameters of the surface via a follow-up training of a regression model. Several regression approaches, such as nearest neighbours, support vector machines, decision trees and ensembles, were trained using scikit-learn [40] and benchmarked, and the most successful algorithms are presented in Table 1. Their accuracy was measured by the average MAE on the latent representations of a test set of simulated CBLEED patterns, and the robustness of the methods is measured through the Coefficient of Determination (R^2) metric, which represents how well unseen examples are likely to be predicted by the model by relating variances in the predictions to variations in the initial inputs. In particular, it is an indication of how predictive the latent representation placements of the CBLEED patterns are for the regression model, and as a consequence — how well new points in the latent space can be quantified.

The methods show a sensitivity of less than 1 eV in predicting the beam energy and less than 0.1 Å with high robustness. The K-nearest Neighbours (KNN) algorithm showed the best robustness and a mean error of 0.43 eV in predicting the Beam Energy in the test examples. The Nu Support Vector Machine (NuSVM) Regression had the best dimer displacement prediction accuracy with a mean error of just 0.01 Å, going well into the sub-angstrom levels of sensitivity.

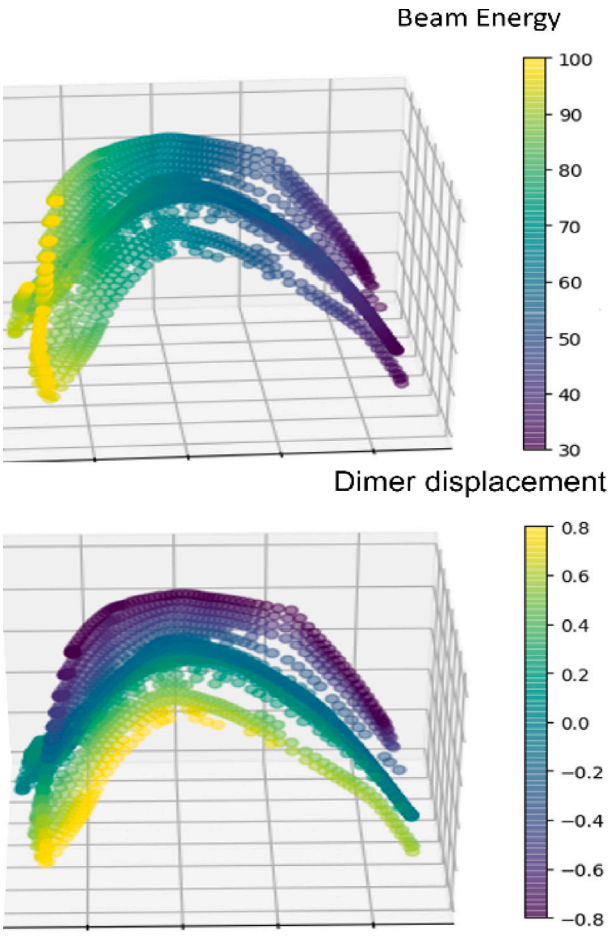

Fig. 6. Latent space structure of the 8-dimensional autoencoder architecture after training. Hessian Locally Linear Embedding [39] is used for dimensionality reduction to three dimensions while preserving the latent space structure. The illustrated data points are from a testing dataset.

4.4. Performance

Training the AE network takes around 1.5 h on an RTX-3080 GPU and i9-11900H CPU machine. Inference from the full pipeline includes a pass of the encoder network to project the image into latent space, and a pass on the regression network to quantify the point. It takes 0.1 sec, giving a processing performance of 10 fps. This performance suggests a quick enough execution time for continuous local inference on a standard lab computer for a real-time structure estimation feed, and alternatively enables instant inference on-demand during an experiment. The performance points towards the suitability of such an algorithm to be trained in advance for an experiment, and be used both in real-time during the experimental run, and after it, to point towards the appropriate structures and enable their confirmation with a single simulations run, rather than a full lengthy exploration of all possibilities in the simulation parameters.

5. Conclusion

A DCAE network was developed and trained on simulated CBLEED patterns, generated with sub-angstrom dimer displacements. The network was shown to be able to generalise the data well with only an 8-dimensional latent space. The well-defined and explainable structure of the latent space is able to learn and identify key physical surface properties and parameters based on the observed CBLEED pattern. The latent space projection of a CBLEED pattern is used to estimate both the beam energy and dimer displacements with high accuracy through secondary regression algorithms, showcasing the ability of the approach to capture multiple parameters at once. With that, the approach is able to provide means of quick and efficient interpretation of a CBLEED pattern, providing a basis for experimental tools for real-time surface structure determination through the CBLEED technique.

The demonstrated approach carries some computational intensity, but even in the relatively narrow use case we used, it mitigates the need for extensive analysis through more straightforward, but laborious approaches that often still rely on simulated data, along with manual inspection methods such as overlaying experimental images, looking for symmetries and other methods that could be applied, in analogue to CBED in STEM. Furthermore, LEEM has been traditionally targeted at a reduced number of material systems due to the limitations on sample properties that allow the use of LEEM imaging. Experiments in standalone LEEM systems are usually aimed at understanding the growth and structural behaviour of one particular material system at a time, and they tend to involve a significant amount of time and resource. Integrating the CBLEED analysis framework proposed here, including the training of the autoencoders for the particular material system under study in this scenario, or scenarios with similar challenges, is feasible and can prove beneficial, enabling real-time analysis during experiments. We believe that the general approach we demonstrate is applicable to a broad range of use cases in microscopy. On a higher level, our results show that relatively simple neural networks are able to interpret this patterns, which is an incentive to make more generalised models on broader data.

CRediT authorship contribution statement

M. Ivanov: Writing – original draft, Visualization, Software, Methodology, Investigation, Data curation, Conceptualization. **J. Pereiro:** Writing – review & editing, Validation, Supervision, Methodology, Investigation, Funding acquisition, Conceptualization.

Declaration of competing interest

The authors declare that they have no known competing financial interests or personal relationships that could have appeared to influence the work reported in this paper.

Data availability

The data used to obtain the results presented in the article are available at https://doi.org/10.17035/cardiff.26652991.

Acknowledgements

The authors acknowledge support from EPSRC research Grants No. EP/P023452/1 and No. EP/ N022661/1 and the National Epitaxy Facility for supplying the samples as part of grant No. EP/ N022661/1. This project also has received funding from the European Union's Horizon 2020 research and innovation programme under the Marie Sklodowska-Curie Grant agreement No. 701246.

References

[1] G. Held, A. Wander, D.A. King, Variations of LEED intensities with angle of incidence and the influence on spot profiles, Phys. Rev. B 51 (1995) 17856–17866.
[2] J.C. Spence, H.C. Poon, D.K. Saldin, Convergent-beam low energy electron diffraction (CBLEED) and the measurement of surface dipole layers, Microscopy Microanal. 10 (2004) 128–133.
[3] B.F. Buxton, J.A. Eades, J.W. Steeds, G.M. Rackham, The symmetry of electron diffraction zone axis patterns, Philos. Trans. R. Soc. London. Series A Math. Phys. Sci. 281 (1976) 171–194.
[4] P. Goodman, A practical method of three-dimensional space-group analysis using convergent-beam electron diffraction, Acta Crystallogr. Sect. A 31 (1975) 804–810.

[5] M. Tanaka, R. Saito, K. Ueno, Y. Harada, Large-angle convergent-beam electron diffraction, J. Electron Microsc. 29 (1980) 408–412, 159.
[6] J.A. Eades, Convergent-beam techniques in transmission electron microscopy, Appl. Surface Sci. 26 (1986) 280–293.
[7] R. Vincent, P.A. Midgley, Double conical beam-rocking system for measurement of integrated electron diffraction intensities, Ultramicroscopy 53 (1994) 271–282, 553.
[8] D.M. Bird, M. Saunders, Sensitivity and accuracy of CBED pattern matching, Ultramicroscopy 45 (1992) 241–251, 68.
[9] J. Zuo, Quantitative convergent beam electron diffraction, Mater. Trans. JIM 39 (1998) 938–946, 60.
[10] K. Tsuda, M. Tanaka, Refinement of crystal structural parameters using two-dimensional energy-filtered CBED patterns, Acta Crystallogr. Sect. A 55 (1999) 939–954, 124.
[11] J.M. LeBeau, S.D. Findlay, L.J. Allen, S. Stemmer, Position averaged convergent beam electron diffraction: Theory and applications, Ultramicroscopy 110 (2010) 118–125, 156.
[12] I. Lazić, E.G. Bosch, S. Lazar, Phase contrast STEM for thin samples: Integrated differential phase contrast, Ultramicroscopy 160 (2016) 265–280, 285.
[13] F.A. Ponce, D. Cherns, W.T. Young, J.W. Steeds, Characterization of dislocations in GaN by transmission electron diffraction and microscopy techniques, Appl. Phys. Lett. 69 (1996) 770–772, 181.
[14] F.A. Ponce, D.P. Bour, W.T. Young, M. Saunders, J.W. Steeds, Determination of lattice polarity for growth of GaN bulk single crystals and epitaxial layers, Appl. Phys. Lett. 69 (1996) 337–339, 221.
[15] H. Kato, K. Miyamoto, M. Sano, T. Yao, Polarity control of ZnO on sapphire by varying the MgO buffer layer thickness, Appl. Phys. Lett. 84 (2004) 4562–4564, 121.
[16] R. Völkl, U. Glatzel, M. Feller-Kniepmeier, Measurement of the lattice misfit in the single crystal nickel based superalloys CMSX-4, SRR99 and SC16 by convergent beam electron diffraction, Acta Mater. 46 (1998) 4395–4404, 112.
[17] J.M. Zuo, M. Kim, M. O'Keefe, J.C.H. Spence, Direct observation of d-orbital holes and cu-cu bonding in Cu2O, Nature 401 (1999) 49–52, 600.
[18] L. Clément, R. Pantel, L.F. Kwakman, J.L. Rouvière, Strain measurements by convergent-beam electron diffraction: The importance of stress relaxation in lamella preparations, Appl. Phys. Lett. 85 (2004) 651–653, 124.
[19] J. Lv, H. Zhang, D. Zhang, L. Liu, Y. Han, Low-dose electron microscopy imaging of electron beam-sensitive crystalline materials, Accounts Mater. Res. 3 (2022) 552–564.
[20] M.S. Altman, Trends in low energy electron microscopy, J. Phys. Condensed Matter 22 (2010).
[21] P.C. Constantinou, D.E. Jesson, On the sensitivity of convergent beam low energy electron diffraction patterns to small atomic displacements, Appl. Surface Sci. 489 (2019) 504–509.
[22] E. Bauer, Low energy electron microscopy, Rep. Progr. Phys. 57 (1994) 895–938.
[23] G. Ruben, D.E. Jesson, D.M. Paganin, A.E. Smith, Kinematic simulation of convergent beam low-energy electron diffraction patterns, Optik 120 (2009) 401–408.
[24] J.M. Ede, Deep learning in electron microscopy, Mach. Learn.: Sci. Technol. 2 (2021).
[25] H. Wang, Y. Xie, D. Li, H. Deng, Y. Zhao, X. Ming, J. Lin, Rapid identification of X-ray diffraction spectra based on very limited data by interpretable convolutional neural networks, J. Mater. Process. Technol. 1 (2018) 1–8.
[26] Y. Suzuki, H. Hino, T. Hawai, K. Saito, M. Kotsugi, K. Ono, Symmetry prediction and knowledge discovery from X-ray diffraction patterns using an interpretable machine learning approach, Sci. Rep. 10 (2020) 1–11.
[27] P.M. Vecsei, K. Choo, J. Chang, T. Neupert, Neural network based classification of crystal symmetries from x-ray diffraction patterns, Phys. Rev. B 99 (2019) 1–9.
[28] F. Oviedo, Z. Ren, S. Sun, C. Settens, Z. Liu, N.T.P. Hartono, S. Ramasamy, B.L. DeCost, S.I. Tian, G. Romano, A.G. Kusne, T. Buonassisi, Fast and interpretable classification of small X-ray diffraction datasets using data augmentation and deep neural networks, npj Comput. Mater. 5 (2019) 1–9.
[29] J.W. Lee, W.B. Park, J.H. Lee, S.P. Singh, K.S. Sohn, A deep-learning technique for phase identification in multiphase inorganic compounds using synthetic XRD powder patterns, Nature Commun. 11 (2020) 1–11.
[30] J. Kwoen, Y. Arakawa, Classification of reflection high-energy electron diffraction pattern using machine learning, Crystal Growth Design 20 (2020) 5289–5293.
[31] J. Kwoen, Y. Arakawa, Multiclass classification of reflection high-energy electron diffraction patterns using deep learning, J. Cryst. Growth 593 (2022) 126780.
[32] K. Kaufmann, C. Zhu, A.S. Rosengarten, D. Maryanovsky, T.J. Harrington, E. Marin, K.S. Vecchio, Crystal symmetry determination in electron diffraction using machine learning, Science 367 (2020) 564–568.
[33] B.H. Martineau, D.N. Johnstone, A.T. van Helvoort, P.A. Midgley, A.S. Eggeman, Unsupervised machine learning applied to scanning precession electron diffraction data, Adv. Struct. Chem. Imaging 5 (2019).
[34] K. Utimula, M. Yano, H. Kimoto, K. Hongo, K. Nakano, R. Maezono, Feature space of XRD patterns constructed by an autoencoder, Adv. Theory Simul. 2200613 (2022).
[35] B.D. Lee, J.-W. Lee, W.B. Park, J. Park, M.-Y. Cho, S.P. Singh, M. Pyo, K.-S. Sohn, Powder X-Ray diffraction pattern is all you need for machine-learning-based symmetry identification and property prediction, Adv. Intell. Syst. 4 (2022) 2200042.
[36] W. Xu, J.M. LeBeau, A deep convolutional neural network to analyze position averaged convergent beam electron diffraction patterns, Ultramicroscopy 188 (2018) 59–69.
[37] C. Zhang, J. Feng, L.R. DaCosta, P.M. Voyles, Atomic resolution convergent beam electron diffraction analysis using convolutional neural networks, Ultramicroscopy 210 (2020) 112921.
[38] D.J. Titterington, C.G. Kinniburgh, Calculation of leed diffracted intensities, Comput. Phys. Comm. 20 (1980) 237–266.
[39] D.L. Donoho, C. Grimes, Hessian eigenmaps: Locally linear embedding techniques for high-dimensional data, Proc. Natl. Acad. Sci. USA 100 (2003) 5591–5596.
[40] F. Pedregosa, G. Varoquaux, A. Gramfort, V. Michel, B. Thirion, O. Grisel, M. Blondel, A. Müller, J. Nothman, G. Louppe, P. Prettenhofer, R. Weiss, V. Dubourg, J. Vanderplas, A. Passos, D. Cournapeau, M. Brucher, M. Perrot, É. Duchesnay, Scikit-learn: Machine learning in python, J. Mach. Learn. Res. 12 (2011) 2825–2830.